Journal of Hydrology 561 (2018) 896–907

Contents lists available at ScienceDirect

Journal of Hydrology

journal homepage: www.elsevier.com/locate/jhydrol

Research papers

Geochemical characteristics of cave drip water respond to ENSO based on a 6-year monitoring work in Yangkou Cave, Southwest China

Chao-Jun Chen[a,b], Ting-Yong Li[a,b,*]

[a] Chongqing Key Laboratory of Karst Environment, School of Geographical Sciences, Southwest University, Chongqing 400715, China
[b] Field Scientific Observation & Research Base of Karst Eco-environments at Nanchuan in Chongqing, Ministry of Land and Resources of China, Chongqing 408435, China

ARTICLE INFO

This manuscript was handled by Corrado Corradini, Editor-in-Chief, with the assistance of Weiping Chen, Associate Editor

Keywords:
Cave drip waters
$\delta^{18}O$ and δD
Mg/Ca
ENSO
Yangkou Cave

ABSTRACT

The scientific explanation of speleothem $\delta^{18}O$ in Chinese monsoon region is a greatly debated issue. Modern cave monitoring combined with instrument observation maybe is an essential solution to deal with this issue. During the period from 2011 to 2016, we monitored local precipitation, soil water in three soil profiles, and six drip water sites in Yangkou Cave, which is located in Chongqing City, Southwest China. This article presents measurements about $\delta^{18}O$, δD and Mg/Ca ratios of drip water and compared these geochemical proxies with contemporaneous atmospheric circulations. The main conclusions are: (1) As water migrates from precipitation to soil water to cave drip water, the amplitudes of seasonal variations in δD and $\delta^{18}O$ decreased gradually. Due to the existence of complex hydrogeological conditions, the range of variation and the seasonal characteristics of δD and $\delta^{18}O$ differ among the drip sites where samples were collected, but the interannual variability is nearly the same. The drip water Mg/Ca ratios are mainly regulated by changes in hydrological conditions in the epikarst zone, with higher values during winter months than that during summer months. (2) When an El Niño event occurs, the Western Pacific Subtropical High (WPSH) is migrated westward, and the production of near-source water vapor from the western Pacific and the South China Sea increases, leading to higher $\delta^{18}O$ values in the precipitation and the cave drip water. The drip water Mg/Ca ratios were significantly lower with increased summer precipitation. On the other hand, during La Niña events, the WPSH is migrated eastward, and inputs of water vapor that has traveled greater distances (from the Indian Ocean) become comparatively important, resulting in lower $\delta^{18}O$ values in the precipitation and the cave drip water. The drip water Mg/Ca ratios were higher with decreased summer precipitation. In summary, the interannual variability of $\delta^{18}O$ in the drip waters of Yangkou Cave reflects changes in water vapor sources caused by atmospheric circulation patterns. Mg/Ca ratios respond to changes of precipitation and CO_2 in soil and can be used to reconstruct abnormal drought or flood events.

1. Introduction

To predict future climate changes, it is especially necessary to recognize the laws that governed past global climate changes. Cave stalagmites, which can be dated with great precision, provide high-resolution records that can be used in paleoclimatic reconstructions (McDermott, 2004; Liu et al., 2013; Duan et al., 2016). Measurements of $\delta^{18}O$ in stalagmites from the Chinese monsoon region record a series of abrupt climate events (Wang et al., 2001). Previous studies have shown that the $\delta^{18}O$ values of stalagmites from the Chinese monsoon region reflect changes in summer precipitation and summer monsoon intensity; more negative $\delta^{18}O$ values in stalagmites indicate stronger summer monsoons, whereas more positive values indicate weaker summer monsoons (Wang et al., 2001, 2005; Cheng et al., 2009; Han et al., 2016; Li et al., 2014, 2017; Zhang et al., 2017). However, the interpretation of the $\delta^{18}O$ signals in Chinese stalagmites is still controversial (Wang and Liu, 2016). Pausata et al., (2011) argued that Chinese stalagmite $\delta^{18}O$ was controlled by Indian monsoon. On the other hand, in the interannual scale, the weakened Indian summer monsoon present anti-phase oscillations with the strengthened East Asian summer monsoon (Hong et al., 2009). Lower $\delta^{18}O$ values do not infer stronger summer monsoons alone (Clemens et al., 2010). Even, others proposed that the variation of $\delta^{18}O$ can primarily reflected local temperature that was dominated by insolation (Dayem et al., 2010).

Maher (2008) noted that the stalagmite records of the monsoon areas in South China and India are consistent. However, these records were inconsistent with other regional precipitation records in China, suggesting that the stalagmites of South China reflect changes in water

* Corresponding author at: School of Geographical Sciences, Southwest University, No. 2 Tiansheng Road, Beibei District, Chongqing 400715, China.
E-mail address: cdlty@swu.edu.cn (T.-Y. Li).

https://doi.org/10.1016/j.jhydrol.2018.04.061
Received 24 January 2018; Received in revised form 19 April 2018; Accepted 25 April 2018
Available online 26 April 2018
0022-1694/

vapor. Tan (2016) argued that the changes in $\delta^{18}O$ in the monsoon region of China are governed by atmospheric circulation patterns over time scales ranging from interannual to centennial or even longer, and these changes mainly reflect the influence of moisture from different source and the ratio of locally derived water vapor to other sources of water vapor in summer monsoon precipitation. Recent stalagmite records from South China indicate that the weakening of the Asian summer monsoon (ASM) is closely tied to El Niño-Southern Oscillation (ENSO) (Burns et al., 2002; Zhao et al., 2016). $\delta^{18}O$ can be influenced by the shifts in the position and intensity of the subtropical pressure cells (Maher and Thompson, 2012). A $\delta^{18}O$ record from a stalagmite collected in Heshang Cave in Hubei province, central China, is one of the strongest pieces of evidence for this assertion. This record has been compared with the Southern Oscillation Index (SOI), and a negative correlation was identified between the two records for the period extending from 1900 to 2000 CE (Fig. 3 in Tan, 2016). Modern instrumental data covering a larger area are critical in the assessment of these views.

Observations in cave drip water contribute to the scientific explanations of speleothem paleoclimate records (Pape et al., 2010). Drip water, which provides the material that forms stalagmites, represents a link between the external environment and cave deposits (Bradley et al., 2010). Much has been learned about the ways in which drip water migrates, the response of drip water to precipitation, and the spatial and temporal changes in the stable isotopes of hydrogen and oxygen through the analysis and monitoring of cave water (Baker et al., 2000; Cobb et al., 2007; Riechelmann et al., 2011; Li et al., 2011; Duan et al., 2016). The changes in $\delta^{18}O$ and the ratios and concentrations of elements in the drip water reflect changes in the climatic environment and the hydrogeological conditions of the epikarst zone (Wackerbarth et al., 2010; Partin et al., 2012; Baldini et al., 2012). For example, the Mg/Ca, δD and $\delta^{18}O$ were sensitive to changes in wet and dry seasons (Partin et al., 2012). Drip rate and CO_2 in cave air may primarily controlled Mg/Ca ratios (Duan et al., 2012). ENSO events also driven drip discharge and hydrogeochemical variations (Tadros et al., 2016), and Moerman et al. (2014) reported that $\delta^{18}O$ variation in precipitation and drip water is sensitivity to ENSO. Cave water has been the primary focus of past studies, whereas less systematic monitoring of precipitation, soil water, and drip water has been conducted (Luo and Wang, 2008; Riechelmann et al., 2017). Fewer studies report the results of continuous monitoring of cave systems (Treble et al., 2013; Genty et al., 2014; Breitenbach et al., 2015; Mattey et al., 2016). Wang et al., (2014) reported the preliminarily monitoring work in Yangkou Cave, only analyzed the seasonal variability of drip water, but not discussed the interannual variability of cave systems. This relative lack of data prevents accurate understanding of the relationship between atmospheric circulation and stable isotopic changes in summer monsoon precipitation and the correct interpretation of the climatic significance of $\delta^{18}O$ records in cave deposits.

Based on six years of δD and $\delta^{18}O$ data from Yangkou Cave, we demonstrate the effects of atmospheric circulation patterns on the stable isotopes of precipitation in the southwest monsoon region of China. We also compare these data with the intensity of ENSO and the WPSH and analyze these atmospheric circulation patterns. The responses of calcium and magnesium in the cave drip waters to external climate changes are also studied. This study advances our understanding of the process by which water migrates from the outside to the inside of caves, based on the chemical indicators it contains.

2. Study area

Yangkou Cave (29°02′N, 107°11′E) is located in Southwest China, specifically in Mount Jinfo of Nanchuan and near the city of Chongqing (Fig. 1a). The study site is located on the southeastern margin of the Sichuan Basin, along the northern margin of the Yun-Gui Plateau and at the northern end of the Dalou Mountains. The uppermost rock unit that makes up Mount Jinfo is Permian limestone, and a huge and complex underground cave system has developed within this unit (Zhang et al., 1998). The cave occurs at an elevation of 2140 m and is 2245 m in length and displays a corridor plane form. The width is generally 15–20 m, and the height is generally 8–12 m. The regional climate is influenced by both the Indian summer monsoon (ISM) and East Asian summer monsoon (EASM) (Fig. 1a, Li et al., 2014). The regional annual mean temperature and annual precipitation is 8.5 °C and 1400 mm, respectively. Precipitation occurs primarily from April to October, when 83% of the annual precipitation occurs, and the annual mean temperature in the cave is 7.5 °C (Zhang et al., 1998; Li et al., 2014). In addition, Han et al., (2016), Zhang et al., (2017) and Li et al., (2017) indicated that the evolution of Asian summer monsoon in the Last Glacial period which reconstructed based on stalagmites from Yangkou Cave, are consistent with other stalagmites records in Chinese monsoon realm including Hulu Cave (Wang et al., 2001), Xiaobailong Cave (Cai et al., 2006), Sanbao Cave (Wang et al., 2008) and Xinya Cave (Li et al., 2007). Series abrupt climatic events, such as Heinrich events, had been dated with higher precise chronology benefit from the high Uranium concentration (~10 ppm) of the stalagmites in Yangkou Cave (Han et al., 2016; Zhang et al., 2017; Li et al., 2017).

3. Data and methods

3.1. Sample collection

Following the collection standards of the International Atomic Energy Agency's Global Network of Isotopes in Precipitation (IAEA-GNIP), we set up a plastic bucket with a funnel and an approximately 1-cm-thick layer of liquid paraffin to collect precipitation outside Yangkou Cave. The bucket was packaged using foil and insulated foam to avoid evaporation of the sample. The bucket and funnel soaked in 5% nitric acid for 24 h were cleaned with deionized water and dried (Chen et al., 2012).

According to the different vegetation and soil conditions at the surface, soil infiltration water was collected at three different locations. SW1#, SW2#, and SW3# were placed at depths of 120 cm, 125 cm and 75 cm in the soil profile, respectively. For each sampling point, a polyethylene (PE) plate for collecting soil water that was 30 cm in diameter was ultrasonically cleaned with deionized water and dried after soaking in 50% hydrochloric acid for 24 h (Fig. 1c, d). The top of the plate was covered with 3 layers of gauze, which had been cleaned and dried by the same method as the plate. Quartz cotton was placed in the layers of the gauze to prevent mud and sand from entering the plate (Fig. 1c). The bottom of the plate was drilled a hole and connected with an external PE bottle with a capacity of 1000 ml through a plastic tube (Fig. 1c, d). One milliliter of $HgCl_2$ solution was added to the bottle to prevent microbial action from affecting the water sample. Each collecting device was positioned horizontally and covered with soil. Because the situations of light precipitation resulted in few soil water, there are several hiatuses in the data of soil water.

We collected drip water at six sites (1#–6#; Fig. 1b) in Yangkou Cave that reflected different distances from the entrance and discharge of the drip water, as well as the height (Wang et al., 2014). Depending on the drip rate, the drip water was collected using 10 ml or 100 ml cylinders; the top of each cylinder had a funnel shape (diameter, 9 cm). The volume of water collected in 1 min was taken to reflect the discharge of the drip water (ml/min), and the drip rates measurements were taken once a month when we visit the cave. Before sampling, all of the vials were soaked in approximately 15% nitric acid for approximately 48 h in the laboratory before being washed with deionized water and dried. At the monitoring sites, the drip water samples were filtered through pre-washed 0.45-μm Millipore nitrocellulose filters, and the bottles were washed with the filtrate; the filtrate was then added to the polyethylene bottles and acidified to pH < 2 through the addition of trace level ultrapure HNO_3 (1:1) for the analysis of the elements Ca and

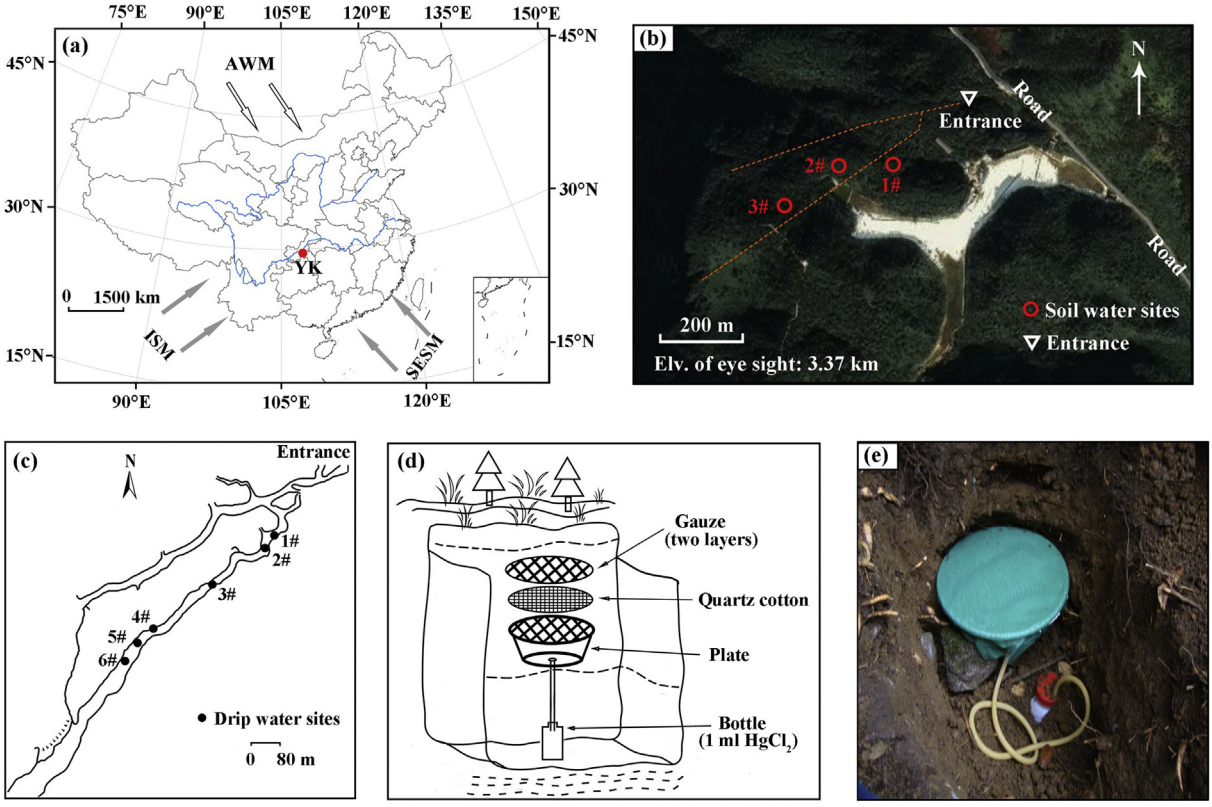

Fig. 1. (a) Location of the study area, Yangkou Cave (YK) in Southwest China. Gray arrows: The Indian summer monsoon (ISM) and the Southeast summer monsoon (SESM). White arrows: The Asian winter monsoon (AWM). The red dot indicates the location of Yangkou Cave. (b) Locations of the soil water sampling sites outside Yangkou Cave. The red dots indicate the soil water sampling sites (1#, 2# and 3#). The brown dashed lines show the extension of Yangkou Cave. (c) Distribution of monitoring sites (black dots) in Yangkou Cave (Black dots are all drip water sites) (modified after Zhang et al., 1998; Wang et al., 2014). (d) and (e) The sketch map for the soil water collector, please see the details in the text. (For interpretation of the references to colour in this figure legend, the reader is referred to the web version of this article.)

Mg. At each site, another 5 ml of filtered drip water was placed in dark brown glass bottles for the measurement of $\delta^{18}O$ and δD. Precipitation and soil water samples were filled over one month, drip water samples were collected instantaneously every month. All of the samples were sealed and kept in a laboratory refrigerator at 5 °C. The monitoring extended from 2011 to 2016. Seasonal sampling was carried out in 2011, whereas samples were collected at regular intervals of one month during the other five hydrological years (2012–2016).

3.2. Sample analyses

All of the measurements were conducted at the School of Geographical Sciences, Southwest University. The stable isotope samples were measured using a DTL-100 liquid water stable isotope analyzer (LWIA) manufactured by Los Gatos Research, USA. 1.5 ml volumes of water were analyzed 6 times, and the average of the last four measurements was taken as the result for a given sample. The results are expressed relative to Vienna Standard Mean Ocean Water (V-SMOW). The accuracy of the measurements is $\leq 0.2‰$ for $\delta^{18}O$ and $\leq 0.5‰$ for δD (Zhou and Li, 2017). The concentrations of Ca and Mg in the drip waters were measured using an Optima 2100DV Inductively Coupled Plasma Optical Emission Spectrometer (ICP-OES) produced by USA. The detection limit is 1 $\mu g\,L^{-1}$, and the relative error of the measurements is less than 2%.

3.3. Cave monitoring and meteorological data

A TESTO 535 infrared CO_2 tester produced in Germany was used to monitor the CO_2 in cave air at the six drip sites. The measurement range of this unit is 0–9999 ppmV, and the testing accuracy is better than 2%.

The precipitation data came from meteorological stations on Mount Jinfo (2250 m a.s.L, 700 m northern of Yangkou Cave) operated by the Meteorological Bureau of Nanchuan. Other data were obtained from the following sources. (1) The Niño 3.4 (5 °S–5 °N, 170 °W–120 °W) Sea Surface Temperature Anomaly (SSTA) index is often used to indicate ENSO events (Dayan et al., 2014), and these data were obtained from http://www.cpc.ncep.noaa.gov/data/indices/sstoi.indices. ENSO events are defined using Niño 3.4 index follow the five consecutive 3-month running mean SST anomalies exceeding 0.5 °C (Kiladis and van Loon, 1988; Abdolrahimi, 2016). According to the United States National Oceanic and Atmospheric Administration (NOAA), a La Niña event occurred from July 2011 to March 2012, and an El Niño event occurred from November 2014 to April 2016. (2) The Western Pacific Subtropical High (WPSH) values (http://cmdp.ncc-cma.net/Monitoring/cn) are used to illustrate the changes in the general circulation pattern associated with ENSO events. (3) The data used to indicate atmospheric circulation patterns were obtained from the daily atmospheric circulation data in Chinese National Climate Center (http://cmdp.ncc-cma.net/Monitoring/cn_stratosphere.php#seasonal) (Jiang et al., 2016). This dataset has a resolution of 2.5° × 2.5°.

4. Results

4.1. Relationship between δD and $\delta^{18}O$ in precipitation

The linear relationship between δD and $\delta^{18}O$ in precipitation is called the meteoric water line (Craig, 1961). According to the measurements of δD and $\delta^{18}O$ in rainwater samples collected outside Yangkou Cave (Fig. 2a), the local meteoric water line (LMWL) is established as $\delta D = 9.0\delta^{18}O + 24.6$ ($n = 57$, $r = 0.99$, $p < 0.01$). This

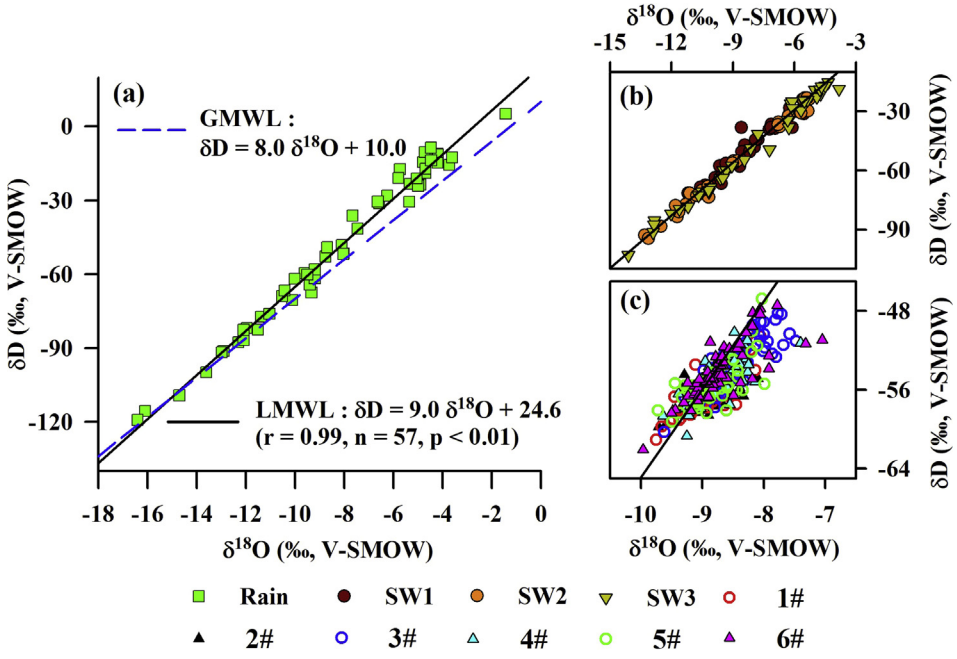

Fig. 2. Relationship between the hydrogen and oxygen isotopic compositions of precipitation, soil water and cave drip water and the local meteoric water line (LMWL). (a) The LMWL (solid black line) based on the $\delta^{18}O$ and δD values of the precipitation measured out Yangkou Cave (green squares). The global meteoric water line (GMWL, dashed blue line; Craig, 1961) has been plotted for comparison. (b) Distribution of $\delta^{18}O$ and δD values of the soil water on the LMWL (black solid line). (c) Distribution of $\delta^{18}O$ and δD values of the drip water on the LMWL (black solid line). (For interpretation of the references to colour in this figure legend, the reader is referred to the web version of this article.)

equation is similar to that established by Wang et al. (2014) for this area ($\delta D = 8.8\delta^{18}O + 22.1$).

The slope and intercept of the LMWL are higher than the global meteoric water line (GMWL) of $\delta D = 8.0\delta^{18}O + 10.0$ (Craig, 1961) because the GMWL represents the combined average of different water and temperature conditions. In contrast, the winter precipitation in the study area is influenced by continental-type air masses, and the winter snowfall leads to higher intercept and slope values (Peng et al., 2007; Kumar et al., 2010). Dansgaard defined deuterium excess (d-excess = δD-$8\delta^{18}O$) (Dansgaard, 1964). The value of d-excess reflects the kinetic fractionation and the climatic conditions in the region (humidity, air temperature, and sea surface temperature of the water vapor) (Tian et al., 2005). The differences of the mean d-excess were less than 2.6‰ between precipitation and soil water and the drip water (Table 1). The $\delta D/\delta^{18}O$ values of the soil water and the drip water collected from the cave are all distributed around the LMWL (Fig. 2b, c), indicating that the collected water samples were not affected by kinetic fractionation. The isotopic compositions of soil water and the drip water respond to the changes in precipitation (Li et al., 2011; Riechelmann et al., 2011).

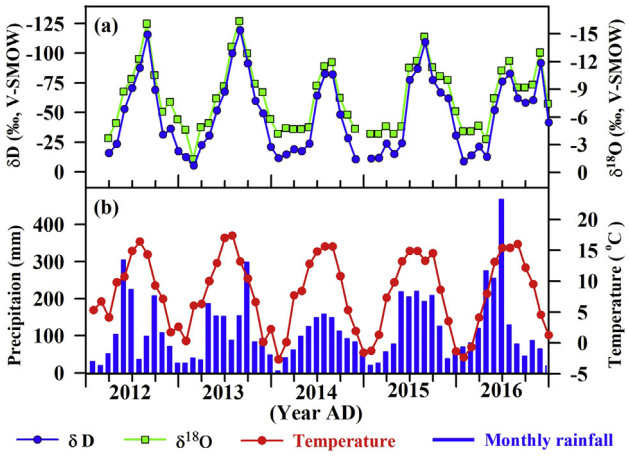

Fig. 3. (a) The monthly variations in the $\delta^{18}O$ (green squares) and δD (blue dots) of precipitation, and (b) the monthly air temperatures (red dots) and amount of precipitation (blue histogram) out Yangkou Cave. It should be noted that the axes of (a) are inverse for a better visibility of the negative correlation with temperature and precipitation. (For interpretation of the references to colour in this figure legend, the reader is referred to the web version of this article.)

4.2. δD and $\delta^{18}O$

During the study period, the range of precipitation $\delta^{18}O$ is −16.4‰ to −1.4‰, and the range of δD is −119.2‰ to −5.2‰, and the mean

Table 1
The maximum, minimum and mean values of δD, $\delta^{18}O$, and d-excess for the precipitation, soil water and drip water in Yangkou Cave.

	δD (‰)			$\delta^{18}O$ (‰)			d-excess (‰)		
	Max.	Mean	Min.	Max.	Mean	Min.	Max.	Mean	Min.
Precipitation	−5.2	−47.8	−119.2	−1.4	−8.1	−16.4	27.2	16.8	7.1
TR1	−24.0	−47.6	−71.6	−5.6	−8.0	−11.2	21.2	16.8	9.9
TR2	−23.4	−58.0	−94.5	−3.0	−8.8	−13.3	20.7	15.7	10.4
TR3	−15.2	−51.5	−116.8	−3.8	−8.5	−16.1	20.0	15.5	8.3
1#	−50.4	−55.8	−61.1	−8.1	−8.9	−9.8	16.8	15.3	10.1
2#	−51.7	−56.1	−59.8	−8.1	−8.9	−9.7	16.9	15.2	9.8
3#	−48.3	−53.5	−60.3	−7.5	−8.5	−9.6	16.0	14.2	8.8
4#	−50.2	−55.1	−60.7	−7.4	−8.8	−9.6	17.3	15.3	8.0
5#	−50.1	−55.6	−59.2	−8.0	−8.9	−9.7	17.6	15.4	8.5
6#	−47.4	−54.1	−62.1	−7.1	−8.7	−10.0	17.6	15.5	5.5

Table 2
The δD and $\delta^{18}O$ values for the summer precipitation out Yangkou Cave.

	2012		2013		2014		2015		2016	
	$\delta^{18}O$ (‰)	δD (‰)	$\delta^{18}O$ (‰)	δD (‰)	$\delta^{18}O$ (‰)	δD (‰)	$\delta^{18}O$ (‰)	δD (‰)	$\delta^{18}O$ (‰)	δD (‰)
June	−10.1	−70.5	−9.3	−67.5	−9.4	−64.2	−11.3	−77.3	−11.0	−76.1
July	−12.3	−87.6	−13.6	−99.8	−11.5	−82.6	−12.1	−86.8	−12.1	−82.6
August	−16.1	−115.6	−16.4	−119.2	−12.0	−81.9	−14.7	−109.3	−9.2	−61.8
Mean	**−12.8**	**−91.2**	−13.1	−95.5	−11.0	−76.2	−12.7	−91.1	**−10.8**	**−73.5**

The mean values of $\delta^{18}O$ and δD for La Niña (2012) and El Niño (2016) years are highlight in bold for contrast.

of $\delta^{18}O$ and δD is −8.1‰ and −47.8‰, respectively, lower than that in the precipitation in Chongqing (Zhou and Li, 2017) (Table 1). $\delta^{18}O$ and δD values of precipitation show obvious seasonal variations; lower values in summer, whereas higher values in winter (Fig. 3). The seasonal variations of $\delta^{18}O$ and δD are negatively correlated with local temperature ($r = -0.58$, $p < 0.01$). In addition, there is also a negative correlation between $\delta^{18}O$ and monthly precipitation ($r = -0.37$, $p < 0.01$). Compared to the summer of 2012, the mean values of $\delta^{18}O$ and δD in the precipitation in the summer of 2016 are 2.0‰ and 17.7‰ higher, respectively (Table 2). The weighted average $\delta^{18}O$ of precipitation during the period from April to October 2016, is −8.7‰, which is 0.8‰ higher compared with that in 2012. The total precipitation from April to October in 2012 and 2016 was 1087 mm and 1340 mm, respectively. On the other hand, the average monthly temperature in the months in 2016 was 1.0 °C higher than that in 2012. This result contradicts the negative correlation between the precipitation $\delta^{18}O$ and precipitation amount and temperature on seasonal time scales.

There is a 1-month lag in the peak of $\delta^{18}O$ and δD values between the soil water and the precipitation (Fig. 4a, a′, b, b′), this should be attributed to the time consuming of infiltration processes of precipitation in soil layers. While, the seasonal variations in $\delta^{18}O$ and δD are generally similar to those of the precipitation (Fig. 4b, b′). The measurements of $\delta^{18}O$ and δD in soil water range from −16.1‰ to −3.0‰ and from −116.8‰ to −15.2‰, respectively. These ranges are slightly less (by 1.8‰ and 12.4‰, respectively) than those measured in the precipitation. The mean value of $\delta^{18}O$ in precipitation and soil water is −8.1‰ and −8.4‰, respectively (Table 1). The slightly lighter for the mean value of $\delta^{18}O$ in soil water than that in precipitation is because of the lack of soil water sample in some months (Fig. 4b), especially in the winter months with higher $\delta^{18}O$ values in precipitation (Fig. 3a). The isotopic values are well define mixing of summer and winter precipitation in soil water samples SW1# and SW#2, moreover sample SW3# is mainly dominated by summer precipitation which lower in $\delta^{18}O$ and δD.

The ranges of $\delta^{18}O$ and δD measurements at the six drip water sites are −10.0‰ to −7.1‰ and −62.1‰ to −47.4‰, respectively. The amplitude for the variation of $\delta^{18}O$ and δD values measured in the drip water are lower by approximately 10.3‰ and 86.9‰, respectively, than the measurements of the same quantities made in the soil water, and lower by approximately 12.1‰ and 99.3‰, respectively, than that in the precipitation. This result clearly reflects mixing of the soil water in the epikarst zone before the formation of the cave drip water (Li et al., 2011; Feng et al., 2014). The values of $\delta^{18}O$ and δD measured in the drip water increase gradually from 2013 to 2016 (Fig. 4). It is similar to the trend of $\delta^{18}O$ and δD variations in precipitation (Fig. 4a).

4.3. Drip rate, CO_2 in cave air, and Mg/Ca ratios

To reduce the occasional errors that may occur in the monitoring process, we discuss only the seasonal mean of each drip rates in this study (winter extends from December to the following February, and summer extends from June to August (Fig. S1 in the Supplementary presents the variation of monthly drip rates). The annual average drip rate at the six cave drip sites are more than 100 ml/min at sites 1# and 2#; 10 ml/min-100 ml/min at sites 3# and 6#; and less than 10 ml/min at sites 4# and 5#. The drip rate at each monitoring site shows seasonal variations (Fig. 5a), and the drip rate in the dry season is slower than that in the rainy season (gray columns in Fig. 5), indicating that the drip rate is mainly controlled by precipitation amount.

The concentrations of cave air CO_2 show a consistent tendency in six monitoring sites. During the wet and warm summer/autumn seasons, the concentrations of CO_2 in the cave is higher than that during the cold and dry winter/spring seasons (Fig. 5b). The annual average CO_2 concentration in the air in Yangkou Cave is 386 ppmV, and the summer average is 489 ppmV. In the summer of 2016, the concentration of CO_2 in cave air (545 ppmV) was higher than the average value and clearly higher than the corresponding value (338 ppmV) in the summer of 2012 (Fig. 5b).

The Mg/Ca ratios measured in the drip water of Yangkou Cave in winter/spring are higher than those measured in summer/autumn in 2011–2016. We used Z-score method to calculate the common variations of Mg/Ca ratios in drip water (Supplementary Fig. S2), reflecting clear seasonal variations (Fig. 5c and Supplementary Fig. S2).

5. Discussion

5.1. $\delta^{18}O$ and δD in precipitation

The negative correlation between $\delta^{18}O$ values and the amount of precipitation above Yangkou Cave is similar to that in other monsoon region in South China (Liu et al., 2008; Li et al., 2010; Zhou and Li, 2017). On the one hand, the negative correlation between $\delta^{18}O$ and temperature and precipitation at this study site is also consistent with the results of monitoring at seven other caves in the monsoon region of China, including Furong Cave in Chongqing, Xianren Cave in Yunnan, and Liangfeng Cave in Guizhou, all are located in Southwest China (Li et al., 2011; Duan et al., 2016). The correlation, however, is contrary to the Rayleigh fractionation that $\delta^{18}O$ is positive with temperature (Dayem et al., 2010), which illustrate that the effect of temperature is negligible. The location of Yangkou Cave is affected by the Asian summer monsoon. During the summer monsoon period, the water vapor mainly comes from the distant Indian Ocean (Ding and Liu, 2008). During the movement of water vapor, precipitation results in the fractionation of the stable isotopes of hydrogen and oxygen (Li et al., 2010; Wang et al., 2014). In summer, during the movement of air masses from the ocean toward the continent, the progressive fallout of precipitation enriched with $\delta^{18}O$ isotopes results in lighter isotopes of the remaining air masses due to isotopic fractionation. In winter, at low humidity and less precipitation amount, the isotopic fractionation during water fall out leading to higher $\delta^{18}O$ values in precipitation (Tian et al., 2005; Cai and Tian, 2016). In combination with these factors, the measurements of $\delta^{18}O$ in the study area decrease in summer and increase in winter.

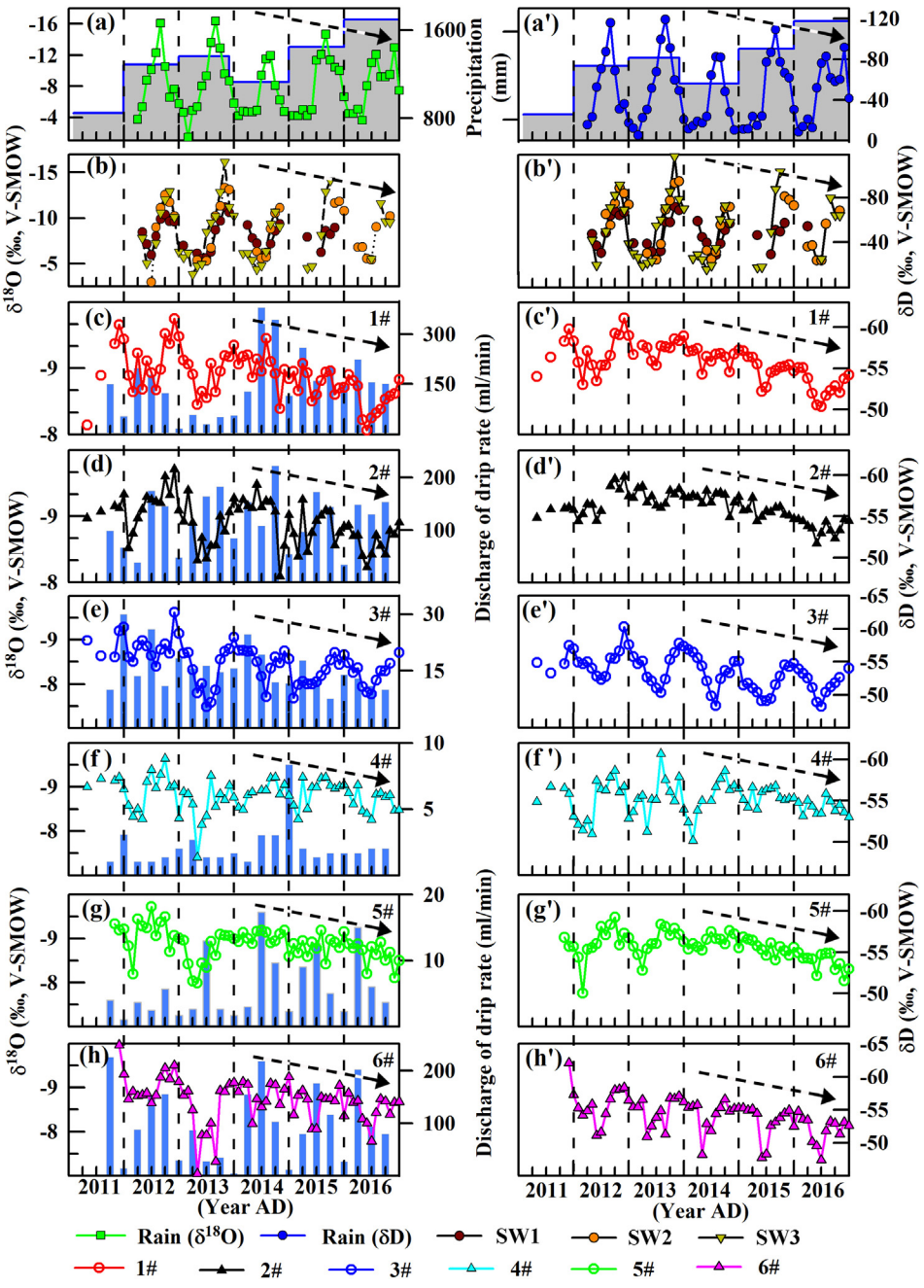

Fig. 4. The monthly variations in the $\delta^{18}O$ (a–h) and δD (a′–h′) of precipitation, soil water and drip water. The blue vertical steps in (a, a′) represents the total of annual precipitation. The blue histograms show the seasonal average discharge for each drip site (c–h). There is a general tendency of higher values for precipitation, soil water and drip water in the change of $\delta^{18}O$ and δD during the monitoring period in this study (dashed lines with arrow). The axes of $\delta^{18}O$ and δD are inverse for a better visibility of the negative correlation with temperature and precipitation. (For interpretation of the references to colour in this figure legend, the reader is referred to the web version of this article.)

5.2. $\delta^{18}O$ and δD in soil water and drip water

Partly because of the absence of soil water samples in some months due to unavoidable circumstances (e.g. no soil water was collected in drought months), there is no correlation between the $\delta^{18}O$ values measured at SW1# and SW2# and $\delta^{18}O$ values measured in the precipitation ($r_{SW1} = 0.07$ and $r_{SW2} = 0.16$) (Table 3). While, the measurements of $\delta^{18}O$ in soil water at SW3# and in the precipitation are strongly correlated ($r = 0.51$, $p < 0.01$) (Table 3). In addition, all the change of the $\delta^{18}O$ values of soil water presented similar seasonal variations as the variations of $\delta^{18}O$ in precipitation (Fig. 4b, b′). Therefore, the $\delta^{18}O$ in soil water inherits the seasonal signals of $\delta^{18}O$ in the precipitation as part of its migration from the atmosphere to the lithosphere.

The variations in $\delta^{18}O$ and δD are similar at drip sites 1# and 2#, which featured with rapid drip rates in annual time scales ($r_{\delta O}^{18} = 0.62$, $r_{\delta D} = 0.78$; $p < 0.01$) (Tables 3 and 4); however, the $\delta^{18}O$ and δD of drip water do not strictly record the interannual variability in $\delta^{18}O$ and δD of the precipitation outside the cave (Fig. 4c, d). The variations in $\delta^{18}O$ and δD are similar at sites 3# and 6#, which featured with moderate drip rates in annual time scales. The seasonal variations are obvious and present a 3- to 6-month lag relative to the precipitation signal (Fig. 4e, 4h). This time lag resulted from the migration of groundwater in the epikarst zone, which varied by the differences in the thickness of overlying host rock and flow path for each drip sites. The lag lead to the phase difference, but it does not change the response of soil water and cave drip water to precipitation. These observations show that the recharge of these drip waters are greatly affected by seasonal precipitation (Baldini et al., 2006). There is a significant correlation between the $\delta^{18}O$ and δD values of drip water at sites 4# and 5#, which featured with slow drip rates ($r_{\delta O}^{18} = 0.52$, $r_{\delta D} = 0.40$, $p < 0.01$) (Tables 3 and 4). However, giving the similar high air humidity (> 95%) in Yangkou Cave, the amplitudes of the $\delta^{18}O$ and δD values measured at site 4# are greater than those at site 5# (Fig. 4f-g, f′-

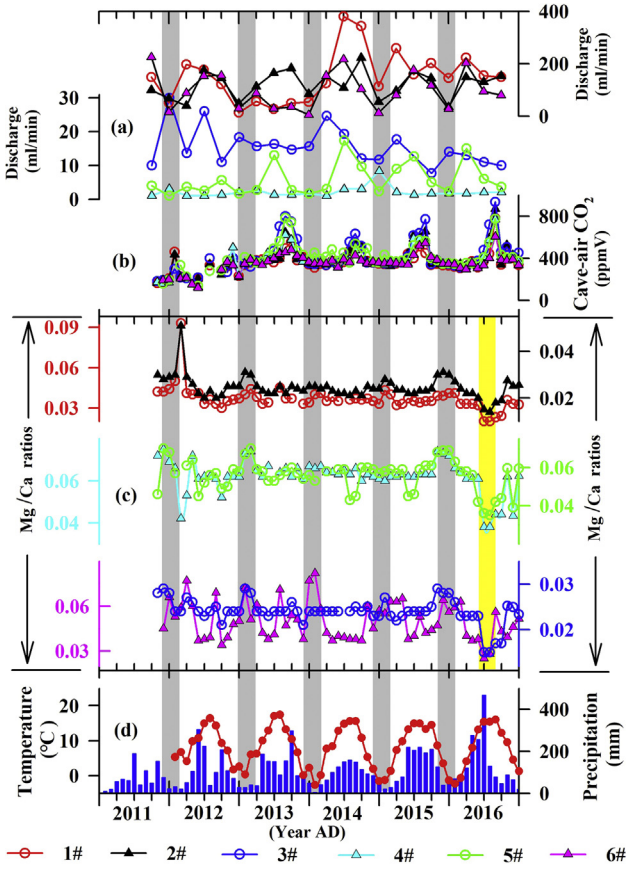

Fig. 5. (a) The changes in the seasonal average discharge at the drip sites in Yangkou Cave (gray columns indicate lower discharges corresponding to drought conditions during the winter and spring months). (b) The P_{CO2} of cave air at the drip sites. (c) The monthly variations in Mg/Ca ratios in drip waters (the yellow column indicate lower Mg/Ca ratios in the months with anomalously high precipitation in 2016). (d) The monthly temperatures (red dots) and precipitation amounts (blue histograms) out Yangkou Cave. (For interpretation of the references to colour in this figure legend, the reader is referred to the web version of this article.)

g′). Because the drip height at site 4# is approximately 10 m, whereas the drip height at site 5# is only approximately 20 cm. The $\delta^{18}O$ and δD values of drip water from site 4# reflects the effects of disequilibrium fractionation during the falling process. In addition, site 5# is located close to an enclosed space within the cave, whereas site 4# is located close to the main tunnel and is affected by the flow of cave air. To sum up, when the seepage flows through the bedrock that hosts the cave, the seepage mixes in the surface karst zone, and the seepage and drip water are homogenized. So, the seasonal variation of the isotopic compositions in the precipitation become attenuated or smoothed (Lambert and Aharon, 2010; Li et al., 2011; Duan et al., 2016). Finally, the amplitude of $\delta^{18}O$ and δD variations decreased from the precipitation to the soil water and subsequently to the drip water. Although the six drip sites in Yangkou Cave display spatial differences in terms of their $\delta^{18}O$ and δD values, the $\delta^{18}O$ values of the six drip sites display the similar general tendency of interannual variability (Fig. 4), and inherited the interannual variability of the stable isotopes in the precipitation (Pape et al., 2010).

5.3. Seasonal variation of Mg/Ca in the drip water

In the monitoring period of 2011–2016, the Mg/Ca ratios of drip water at the six drip water sites in Yangkou Cave present some seasonal variations with higher values in winter and lower values in summer (Fig. 5 and Supplementary Fig. S2). Cave drip water is affected by many factors, such as differences in the surface vegetation cover, the thickness of the overlying carbonate rock, and the flow path, resulting differences in discharge of the drip water and the drip rate (Johnson et al., 2006; Li et al., 2011; Casteel and Banner, 2015). Tooth and Fairchild (2003) noted that the evolution of Mg/Ca ratios reflect hydrological changes from dry to wet conditions and vice versa, and Mg/Ca ratios in cave drip water are affected by precipitation (which is the source of karst water), prior calcite precipitation (PCP), and the leaching of the overlying soil. Carbon dioxide (CO_2) is the main factor controlling the dissolution of karst rocks which produced from atmospheric and soil CO_2. The CO_2 gas dissolve in precipitation and soil water, forming carbonic acid (lowering the pH value) which can dissolve carbonate rocks, such as calcite ($CaCO_3$) and dolomite ($CaMg(CO_3)_2$), during infiltration through soil layers (Cai et al., 2011). The ratio of Mg/Ca in cave drip water depends on the rate of dissolution of carbonate rocks which is higher in calcite than dolomite rocks. In the winter and spring months, precipitation outside Yangkou Cave is limited (Fig. 5d), the drip rate is slow (Fig. 5a), CO_2 percentage is low compared to summer season, so the rate of dissolution of carbonate rock decrease. During dry season (the winter months), the pathway of groundwater may relatively open in the epikarst zone which were conductive to the degassing of CO_2 from the infiltration water, thus causing more Ca to precipitate along a flow path (Fairchild et al., 2000; Partin et al., 2012), and finally resulted in higher Mg/Ca in drip water. Conversely during the summer, low Mg/Ca ratio is the result of increasing rate of calcite dissolution, enriched calcium ions in drip water.

The concentration of CO_2 in cave air is also an important factor that may influence the degassing of CO_2 and Mg/Ca ratios (Spötl et al., 2005; Johnson et al., 2006). In general, CO_2 in cave air may come from soil bio-productivity, decomposition of organic material in soil and cave, and geothermal activity (Baldini et al., 2008). The concentration of CO_2 in caves is mainly controlled by the rate of input of CO_2 from the overlying soil (Wong and Banner, 2010; Cowan et al., 2013). High concentrations of CO_2 in the cave air prevents the degassing of CO_2

Table 3
Correlations between the monthly $\delta^{18}O$ values of the drip water, soil water, and precipitation.

r	1#	2#	3#	4#	5#	6#	TR1	TR2	TR3
2#	0.62**								
3#	0.39**	0.54**							
4#	0.40**	0.54**	0.20						
5#	0.15	0.20	0.24*	0.52**					
6#	0.50**	0.36**	0.52**	0.33**	0.26*				
TR1	0.28	0.33	0.56**	0.43**	0.17	0.35			
TR2	0.38*	0.48**	0.48**	0.60**	0.16	0.34	0.93**		
TR3	0.14	0.24	0.22	0.39*	0.22	0.28	0.71**	0.87**	
Precipitation	−0.11	0.02	−0.20	0.35**	0.05	−0.11	0.07	0.16	0.51**

* Indicates significant at a 95% confidence level ($p < 0.05$).
** Indicates significant at a 99% confidence level ($p < 0.01$).

Table 4
Correlations between monthly δD values of the drip water, soil water, and precipitation.

r	1#	2#	3#	4#	5#	6#	TR1	TR2	TR3
2#	0.78**								
3#	0.64**	0.46**							
4#	0.21	0.34**	−0.12						
5#	0.41**	0.38**	0.07	0.40**					
6#	0.77**	0.53**	0.69**	0.15	0.21				
TR1	0.48**	0.38*	0.79**	0.14	0.19	0.60**			
TR2	0.49**	0.38*	0.81**	0.30	0.36	0.67**	0.88**		
TR3	0.26	0.13	0.31	0.39*	0.29	0.46**	0.65**	0.80**	
Precipitation	0.14	−0.03	−0.32	0.51**	0.16	−0.14	−0.05**	−0.03	0.48**

* Indicates significant at a 95% confidence level ($p < 0.05$).
** Indicates significant at a 99% confidence level ($p < 0.01$).

from the drip water, resulting in lower calcite deposition precipitation (Cai et al., 2011). At the same time, the drip speed increased in summer/autumn and karst fissure were filled with water, which is not conducive to the degassing of CO_2 from interstitial water in the flow (Sherwin and Baldini, 2011; Partin et al., 2012). Thus, the precipitation of $CaCO_3$ is inhibited, which further results in lower Mg/Ca ratios (Baldini et al., 2008).

5.4. The $\delta^{18}O$, δD and Mg/Ca ratios respond to ENSO and atmospheric circulation

The values of $\delta^{18}O$ and δD measured in the drip water increase gradually from 2013 to 2016 (Fig. 4). Moreover, the values of $\delta^{18}O$ and δD measured in the precipitation also tend to be heavier in summer after 2013 (Fig. 4a). The lowest value of precipitation $\delta^{18}O$ and δD in the summer of 2016 is 4.0‰ and 33.6‰ higher than that in the summer of 2012, respectively (Fig. 4a). This result contradicts the negative correlation between the $\delta^{18}O$ in the precipitation and precipitation amount and temperature in seasonal scales (section 4.2). We suggest that the "inverse precipitation effect" seen in the interannual scale is due to the circulation effect, which proposed that the variation of atmosphere circulation changed the moisture source and finally resulted in the change of precipitation $\delta^{18}O$ (Tan, 2014, 2016).

Changes in the $\delta^{18}O$ and δD values measured in precipitation in interannual time scales can reflect climatic changes on large spatial scales (Cobb et al., 2007; Mischel et al., 2015) and are influenced by the global pattern of atmospheric circulation (Lambert and Aharon, 2010). Water vapor in the summer monsoon region of China is primarily derived from three sources: (1) the Indian Ocean (via the Southwest summer monsoon); (2) the South China Sea; (3) the tropical western Pacific (via the Southeast summer monsoon) (Tian et al., 2004; Sun et al., 2006; Liu et al., 2008). In the summer of 2012, during the decay of the La Niña (Kiladis and van Loon, 1988; Trenberth, 1997; Zhou and Li, 2017), the WPSH was located northern and eastern of the average position, its area decreased, and the value of the main area of the WPSH showed a negative anomaly relative to the average (Fig. 6a). A cyclonic circulation pattern developed in the western North Pacific (a western North Pacific cyclone or a WNPC) and the eastern coast of China, and anomalous west winds occurred at lower latitudes (Fig. 6b) (Chen et al., 2013). The water vapor was mainly derived from the Indian Ocean, and a divergence formed in Southwest China (Fig. 6c). At the same time, the amount of precipitation falling within the study area decreased (Fig. 6c). The long distance of water vapor led to lower $\delta^{18}O$ values (Breitenbach et al., 2010; Tan, 2014). In another hand, the northerly winds in the western WNPC blocked the water vapor from the western Pacific Ocean from reaching the inland areas. The southeast monsoon became weak in the following summer (Zhou et al., 2014), and the input of water vapor from the local source (the Pacific Ocean) during the summer monsoon precipitation period decreased (Fig. 6c) (Tan, 2014, 2016).

During the El Niño event, convective cooling over the tropical western Pacific Ocean caused the tropical atmosphere to produce a Rossby wave in the lower troposphere (Cai et al., 2017), resulting in the development of anomalous anticyclonic circulation in the western North Pacific (a western North Pacific anticyclone or a WNPAC) (Fig. 6e) (Cai et al., 2017). The southeast monsoon was enhanced, and the precipitation in the Yangtze River drainage area increased in the summer of the following year (Fig. 6f) (Zhang et al., 1999). In the summer of 2016, during the decay of the El Niño, the WPSH was located to the west of the past average position, a ridge was located to the south, and the area of the WPSH increased (Fig. 6d); moreover, a large portion of the WPSH area showed positive anomalies (Fig. 6d). Thus, the intensity of the WPSH in 2016 was clearly stronger than that of 2012 (Fig. 6a, d) (Jiang et al., 2016). Anomalous east winds developed at low latitudes, and an anticyclonic circulation pattern (WNPAC) appeared over the eastern coast of China (Fig. 6e) (Cai et al., 2017). The inputs of water vapor from the western Pacific Ocean and the South China Sea increased and the water vapor displayed convergence (green shading), resulting in the increase of precipitation over the study area (Fig. 6f).

Tan (2014, 2016) argued that moisture source from the western Pacific Ocean and the South China Sea led to higher $\delta^{18}O$ values and the $\delta^{18}O$ value of rainwater didn't depend on the precipitation sum. Cai and Tian (2016) demonstrate that at the situation of El Niño, the Walker circulation is weakened, and the convective intensity in Indo-Pacific region is weak, resulting in less precipitation and inhibits the fractionation of isotope in precipitation, and finally leads to higher values of $\delta^{18}O$. So, they proposed that precipitation $\delta^{18}O$ in ASM region is not strongly related to change of moisture source (Cai et al., 2017). However, based on four caves monitoring work in the Asian monsoon region and combined with the analysis of IsoGSM model, Yang et al. (2016) confirmed that the values of $\delta^{18}O$ in precipitation were enhanced during El Niño period. In the same time, the annual weighted average of precipitation $\delta^{18}O$ and δD values in 2016 is 0.6‰ and 6.5‰ higher, respectively, compared to that in 2012 at Hong Kong site (data come from the International Atomic Energy Agency website). These changes were also noted by Moerman et al. (2013, 2014) in the study of the caves in Borneo (4°N, 114°E), Malaysia. Finally, based on our cave monitoring results and the analysis of atmospheric circulation (Fig. 6), we proposed that change of moisture source can significantly influence on the $\delta^{18}O$ of precipitation and drip water, with higher values during El Niño and lower values during La Niña periods, respectively. This is consistent with previous hypothesis that the values of $\delta^{18}O$ in precipitation responds to ENSO within most parts of the monsoon region of China (Ishizaki et al., 2012; Tan, 2014).

McDonald et al. (2004) demonstrated that Mg/Ca ratios in drip water can response to ENSO events based on the monitoring work in Wombeyan Cave. Tadros et al. (2016) shown that the variation of Mg/Ca ratios in drip water is opposite between El Niño event and La Niña event. In this study, the change in Mg/Ca in drip water was increase

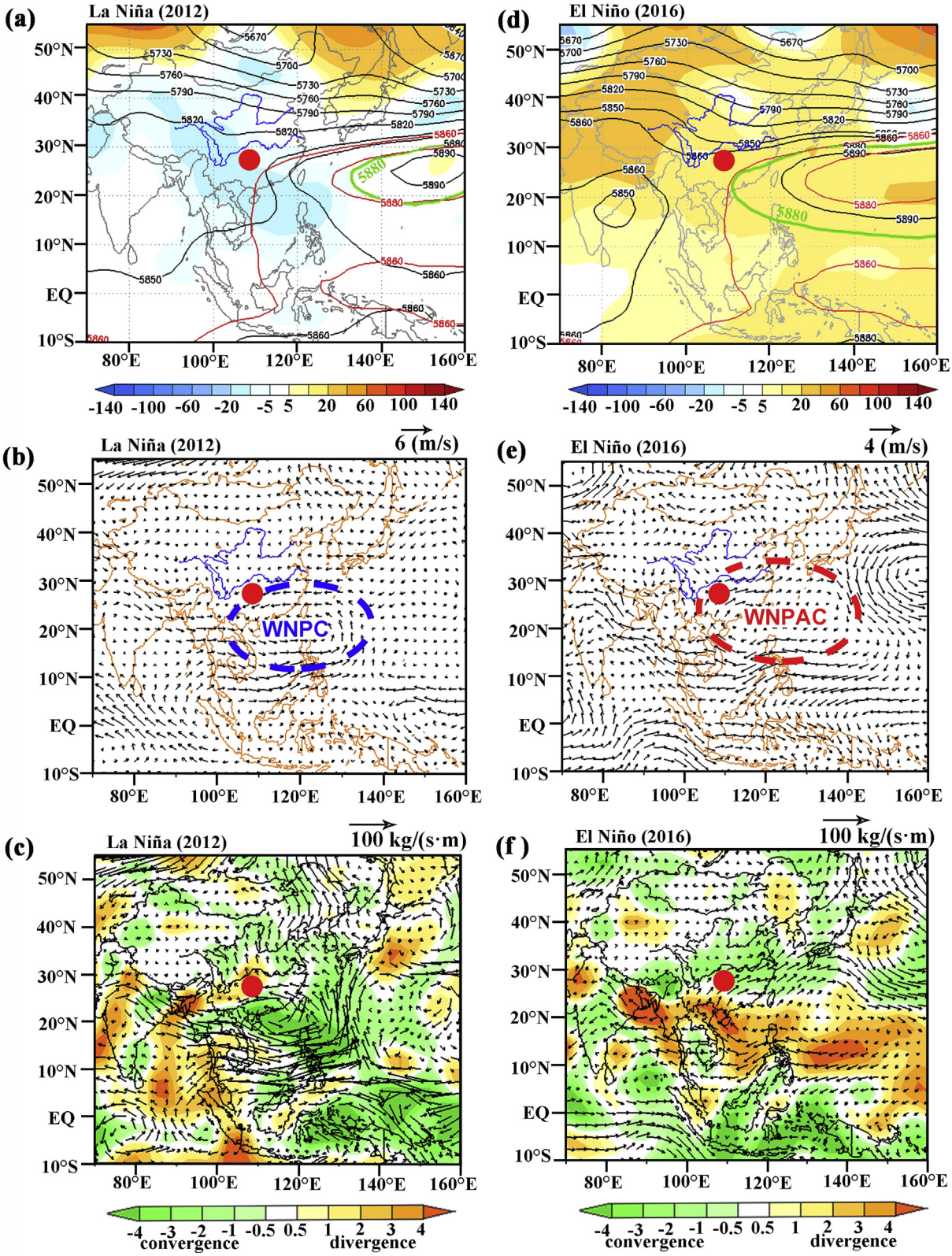

Fig. 6. Averaged atmospheric circulation anomalies in June–July (modified after Yuan et al., 2017). (a, d) 500-hPa geopotential height (contours) and anomalies (shading) (Jiang et al., 2016). Green 5880 contours represent the Western Pacific Subtropical High (WPSH) in 2012 (a) and 2016 (d), respectively (unit: gpm). Red contours indicate the average WPSH during 1981–2010. Colors from white to red in the scale represent positive anomalies (unit: gpm). The WPSH moved distinctly westward in 2016, in contrast to its average position. (b, e) 850-hPa wind anomalies (unit: m/s). The dashed blue ellipse in Fig. 6b indicates the western North Pacific cyclone (WNPC), and the red dashed ellipse in Fig. 6e indicates the western North Pacific anticyclone (WNPAC) (Chen et al., 2013; Cai et al., 2017). (c, f) Anomalous moisture flux integrated from 1000 hPa to 300 hPa (vectors; unit: kg/(m*s)) and divergence (shading; unit: 10^{-5} kg/(m^2*s)) (Yuan et al., 2017). The red dots indicate the location of Yangkou Cave. In 2012, Yangkou Cave was located in a divergence zone, and the local rainfall decreased. In contrast, in 2016, Yangkou Cave was located in a convergence zone, and the local rainfall increased. (For interpretation of the references to colour in this figure legend, the reader is referred to the web version of this article.)

slightly in the summer of 2012 (Supplementary Fig. S2), the decay period of the La Niña event discussed above, but was significantly lower in the summer of 2016 (Fig. 5c and Supplementary Fig. S2), during the decay of the El Niño event. The precipitation in the study area increased in El Niño event because the major rainbelt of China is concentrated in the middle and lower reaches of the Yangtze River during El Niño event (Wang et al., 2015). The slightly increase of Mg/Ca ratios in drip water in the summer of 2012 corresponds to an abnormal decrease in precipitation during July and August of that year, which is normally 359 mm (based on the data from Chongqing meteorological bureau, 1970–2000), but as less as 136 mm in the July and August of 2012 (Fig. 5d). This abnormal decrease in summer rainfall resulted in an increase in the time available for water–rock interactions, finally leading to increases in the Mg/Ca ratios (Musgrove and Banner, 2004). In addition, the higher Mg/Ca ratios values of drip water in the summer of 2013 also respond to the decrease in precipitation in July of 2013 (Fig. S2).

The Mg/Ca ratios of the drip water collected in the summer of 2016 are clearly low (Fig. 5c, Supplementary Fig. S2), which is consistent with the abnormal increase in precipitation that occurred from April to June in 2016 (Fig. 5d). Increases in precipitation lead to increases in the velocity of water infiltration into soil and epikarst zone, and shorten the contact time between soil/rock and water (Fairchild et al., 2000; Li et al., 2013). Because the dissolution rate of calcite is greater than that of dolomite (Chou et al., 1989), the Mg concentrations decrease to a greater degree than the Ca concentrations during the summer of 2016, resulting in significantly smaller Mg/Ca ratios. This deduction has been confirmed by the change of Mg and Ca concentrations measured in drip water. The concentrations of Mg and Ca in the drip water were significantly lower in the summer of 2016 than in 2012. The Ca concentrations measured at the six drip water sites decreased by 10–31%; the decrease in the measured Mg concentrations was 44–54%. The Mg concentrations decrease to a greater degree than the Ca concentrations. These observations confirm that Mg/Ca ratios can respond to abnormal precipitation events (e.g., seasonal drought or flood events).

In addition, warm and humid surface environments enhanced the soil biological effect (Bond-Lamberty and Thomson, 2010), the strengthened respiration and decomposition in soil release more CO_2 and increased the CO_2 concentration in cave air (Fig. 5b). A rise in P_{CO2} in cave air inhibits the CO_2 degassing from drip water (Duan et al., 2012), depressed the deposition of carbonate from drip water, which also contributes to lower Mg/Ca ratios.

In summary, in the interannual time scales, the change of $\delta^{18}O$ and δD in drip water in ASM regions is dominated by the change of atmospheric circulation, such as the variation of ENSO situations. While, the Mg/Ca ratios in cave drip water responded to the change of CO_2 in soil and the external hydrological conditions. Thus, they can be used as indicators in the reconstruction of paleoclimate. Although other factors as PCP can cause the rising of Mg/Ca ratios in drip water, the occurrence of PCP is essentially influenced by hydrological conditions which mainly dominated by precipitation.

6. Conclusions

(1) Measurements of $\delta^{18}O$ and δD in precipitation falling on Mount Jinfo show significant seasonal changes and negative correlations with temperature and precipitation. Although the epikarst zone contains a mixture of precipitation from different times of the year, the obvious seasonal and interannual changes in $\delta^{18}O$ and δD in the soil water and drip water respond to precipitation on interannual scale. Measurements of $\delta^{18}O$ in the drip water can reflect the $\delta^{18}O$ signal in precipitation.

(2) The changes in $\delta^{18}O$ and δD in precipitation are closely related to the atmospheric circulation patterns on interannual time scales in the area of Yangkou Cave. During El Niño events, the WPSH is stronger and located farther west; the southwest monsoon is weaker, whereas the southeast monsoon is stronger; and the inputs of water vapor from the nearby source in the western Pacific increase. Finally, the $\delta^{18}O$ of the precipitation is higher values. During La Niña events, the WPSH shrinks and is located farther east; the southwest monsoon is enhanced; the water vapor is derived primarily from the Indian Ocean; and the $\delta^{18}O$ of the precipitation is lower values.

(3) Mg/Ca ratios can reflect changes of CO_2 in soil and hydrological conditions in epikarst zones which dominated by the precipitation that falls outside of cave. When the precipitation and CO_2 in soil anomaly increases in summer, the Mg/Ca ratios decrease in the drip water; when the summer precipitation and CO_2 in soil decreases, the Mg/Ca ratios increase in the drip water.

Acknowledgement

The editor Corrado Corradini and three anonymous reviewers are greatly appreciated for their constructive comments to improve the quality of this article. This research was supported by grants from the National Natural Science Foundation of China (NSFC; No. 41772170) and the Fundamental Research Funds for the Central Universities (Nos. XDJK2017A010 and XDJK2013A012) to T.-Y. Li.

Appendix A. Supplementary data

Supplementary data associated with this article can be found, in the online version, at http://dx.doi.org/10.1016/j.jhydrol.2018.04.061.

References

Abdolrahimi, M., 2016. The Effect of El Niño Southern Oscillation (ENSO) on World Cereal Production (Master's thesis). University of Sydney.
Baker, A., Genty, D., Fairchild, I.J., 2000. Hydrological characterisation of stalagmite drip waters at Grotte de Villars, Dordogne, by the analysis of inorganic species and luminescent organic matter. Hydrol. Earth Syst. Sci. 4 (3), 439–449.
Baldini, J.U., McDermott, F., Baldini, L.M., Ottley, C.J., Linge, K.L., Clipson, N., Jarvis, K.E., 2012. Identifying short-term and seasonal trends in cave drip water trace element concentrations based on a daily-scale automatically collected drip water dataset. Chem. Geol. 330, 1–16.
Baldini, J.U.L., McDermott, F., Fairchild, I.J., 2006. Spatial variability in cave drip water hydrochemistry: implications for stalagmite paleoclimate records. Chem. Geol. 235 (3), 390–404.
Baldini, J.U.L., McDermott, F., Hoffmann, D.L., Richards, D.A., Clipson, N., 2008. Very high-frequency and seasonal cave atmosphere P_{CO2} variability: implications for stalagmite growth and oxygen isotope-based paleoclimate records. Earth Planet. Sci. Lett. 272 (1), 118–129.
Bond-Lamberty, B., Thomson, A., 2010. Temperature-associated increases in the global soil respiration record. Nature 464 (7288), 579.
Bradley, C., Baker, A., Jex, C.N., Leng, M.J., 2010. Hydrological uncertainties in the modelling of cave drip-water $\delta^{18}O$ and the implications for stalagmite palaeoclimate reconstructions. Quatern. Sci. Rev. 29 (17), 2201–2214.
Breitenbach, S.F., Adkins, J.F., Meyer, H., Marwan, N., Kumar, K.K., Haug, G.H., 2010. Strong influence of water vapor source dynamics on stable isotopes in precipitation observed in Southern Meghalaya, NE India. Earth Planet. Sci. Lett. 292 (1), 212–220.
Breitenbach, S.F., Lechleitner, F.A., Meyer, H., Diengdoh, G., Mattey, D., Marwan, N., 2015. Cave ventilation and rainfall signals in drip water in a monsoonal setting–a monitoring study from NE India. Chem. Geol. 402, 111–124.
Burns, S.J., Fleitmann, D., Mudelsee, M., Neff, U., Matter, A., Mangini, A., 2002. A 780-year annually resolved record of Indian Ocean monsoon precipitation from a speleothem from south Oman. J. Geophys. Res. 107 (D20), 4434.
Cai, B., Zhu, J., Ban, F., Tan, M., 2011. Intra-annual variation of the calcite deposition rate of drip water in Shihua Cave, Beijing, China and its implications for palaeoclimatic reconstructions. Boreas 40 (3), 525–535.
Cai, Y.-J., An, Z.-S., Cheng, H., Edwards, R.L., Kelly, M.J., Liu, W.-G., Shen, C.-C., 2006. High-resolution absolute-dated Indian Monsoon record between 53 and 36 ka from Xiaobailong Cave, southwestern China. Geology 34 (8), 621–624.
Cai, Z., Tian, L., 2016. Atmospheric controls on seasonal and interannual variations in the precipitation isotope in the East Asian monsoon region. J. Climate 29 (4), 1339–1352.
Cai, Z., Tian, L., Bowen, G.J., 2017. ENSO variability reflected in precipitation oxygen isotopes across the Asian Summer Monsoon region. Earth Planet. Sci. Lett. 475, 25–33.
Casteel, R.C., Banner, J.L., 2015. Temperature-driven seasonal calcite growth and drip water trace element variations in a well-ventilated Texas cave: Implications for speleothem paleoclimate studies. Chem. Geol. 392, 43–58.
Chen, H.-L., Li, T.-Y., Zhou, F.-L., Peng, L.-L., Li, J.-Y., 2012. Analysis of chemical

characteristics of meteoric precipitation based on the data of a series of rainwater——a case study of southwest university, Beibei district, Chongqing. J. Southwest Univ. 34 (2), 105–113 (in Chinese with English abstract and figures).
Chen, W., Feng, J., Wu, R., 2013. Roles of ENSO and PDO in the link of the East Asian winter monsoon to the following summer monsoon. J. Climate 26 (2), 622–635.
Cheng, H., Edwards, R.L., Broecker, W.S., Denton, G.H., Kong, X., Wang, Y., Zhang, R., Wang, X., 2009. Ice age terminations. Science 326 (5950), 248–252.
Chou, L.E.I., Garrels, R.M., Wollast, R., 1989. Comparative study of the kinetics and mechanisms of dissolution of carbonate minerals. Chem. Geol. 78 (3–4), 269–282.
Clemens, S.C., Prell, W.L., Sun, Y., 2010. Orbital-scale timing and mechanisms driving Late Pleistocene Indo-Asian summer monsoons: reinterpreting cave speleothem $\delta^{18}O$. Paleoceanography 25 (4), 545–558.
Cobb, K.M., Adkins, J.F., Partin, J.W., Clark, B., 2007. Regional-scale climate influences on temporal variations of rainwater and cave drip water oxygen isotopes in northern Borneo. Earth Planet. Sci. Lett. 263 (3), 207–220.
Cowan, B.D., Osborne, M.C., Banner, J.L., 2013. Temporal variability of cave-air CO_2 in central Texas. J. Cave Karst Stud. 75 (1), 38–50.
Craig, H., 1961. Isotopic variations in meteoric waters. Science 133 (3465), 1702–1703.
Dansgaard, W., 1964. Stable isotopes in precipitation. Tellus 16 (4), 436–468.
Dayan, H., Vialard, J., Izumo, T., Lengaigne, M., 2014. Does sea surface temperature outside the tropical Pacific contribute to enhanced ENSO predictability? Clim. Dynam. 43 (5–6), 1311–1325.
Dayem, K.E., Molnar, P., Battisti, D.S., Roe, G.H., 2010. Lessons learned from oxygen isotopes in modern precipitation applied to interpretation of speleothem records of paleoclimate from eastern Asia. Earth Planet. Sci. Lett. 295 (1), 219–230.
Ding, Y.H., Liu, Y.Y., 2008. A study of the teleconnections in the Asian-Pacific monsoon region. Acta Meteor Sinica 22 (4), 404–418 (In Chinese).
Duan, W., Cai, B., Tan, M., Liu, H., Zhang, Y., 2012. The growth mechanism of the aragonitic stalagmite laminae from Yunnan Xianren Cave, SW China revealed by cave monitoring. Boreas 41 (1), 113–123.
Duan, W., Ruan, J., Luo, W.J., Li, T.-Y., Tian, L., Zeng, G., Zhang, D., Bai, Y., Li, J., Tao, T., Zhang, P., Baker, A., Tan, M., 2016. The transfer of seasonal isotopic variability between precipitation and drip water at eight caves in the monsoon regions of China. Geochim. Cosmochim. Acta 183, 250–266.
Duan, W., Cheng, H., Tan, M., Edwards, R.L., 2016. Onset and duration of transitions into Greenland Interstadials 15.2 and 14 in northern China constrained by an annually laminated stalagmite. Sci. Rep. 6 (20844). http://dx.doi.org/10.1038/srep20844.
Fairchild, I.J., Borsato, A., Tooth, A.F., Frisia, S., Hawkesworth, C.J., Huang, Y., McDermott, F., Spiro, B., 2000. Controls on trace element (Sr–Mg) compositions of carbonate cave waters: implications for speleothem climatic records. Chem. Geol. 166 (3), 255–269.
Feng, W., Casteel, R.C., Banner, J.L., Heinze-Fry, A., 2014. Oxygen isotope variations in rainfall, drip-water and speleothem calcite from a well-ventilated cave in Texas, USA: assessing a new speleothem temperature proxy. Geochim. Cosmochim. Acta 127, 233–250.
Genty, D., Labuhn, I., Hoffmann, G., Danis, P.A., Mestre, O., Bourges, F., Orengo, P., 2014. Rainfall and cave water isotopic relationships in two South-France sites. Geochim. Cosmochim. Acta 131, 323–343.
Han, L.-Y., Li, T.-Y., Cheng, H., Edwards, R.L., Shen, C.-C., Li, H.-C., Huang, C.-X., Li, J.-Y., Yuan, N., Wang, H.-B., Zhang, T.-T., Zhao, X., 2016. Potential influence of temperature changes in the Southern Hemisphere on the evolution of the Asian summer monsoon during the last glacial period. Quat. Int. 392, 239–250.
Hong, Y.T., Hong, B., Lin, Q.H., Shibata, Y., Zhu, Y.X., Leng, X.T., Wang, Y., 2009. Synchronous climate anomalies in the western North Pacific and North Atlantic regions during the last 14,000 years. Quatern. Sci. Rev. 28 (9), 840–849.
Ishizaki, Y., Yoshimura, K., Kanae, S., Kimoto, M., Kurita, N., Oki, T., 2012. Interannual variability of $H_2{}^{18}O$ in precipitation over the Asian monsoon region. J. Geophys. Res. 117 (D16).
Jiang, W., Zhang, Z., Liu, Y., 2016. Relationship between the dry-season precipitation in Southwest China and decadal changes of the western pacific subtropical high since the 21st century. Meteor. Mon. 42 (11), 1335–1341 (in Chinese with English abstract and figures).
Johnson, K.R., Hu, C., Belshaw, N.S., Henderson, G.M., 2006. Seasonal trace-element and stable-isotope variations in a Chinese speleothem: the potential for high-resolution paleomonsoon reconstruction. Earth Planet. Sci. Lett. 244 (1), 394–407.
Kiladis, G.N., van Loon, H., 1988. The Southern Oscillation. Part VII: Meteorological anomalies over the Indian and Pacific sectors associated with the extremes of the oscillation. Monthly Weather Rev. 116, 120–136.
Kumar, B., Rai, S.P., Kumar, U.S., Verma, S.K., Garg, P., Kumar, S.V., Jaiswal, R., Purendra, B.K., Kumar, S.R., Pande, N.G., 2010. Isotopic characteristics of Indian precipitation. Water Resour. Res. 46 (12), 1–15 W12548.
Lambert, W.J., Aharon, P., 2010. Oxygen and hydrogen isotopes of rainfall and dripwater at DeSoto Caverns (Alabama, USA): Key to understanding past variability of moisture transport from the Gulf of Mexico. Geochim. Cosmochim. Acta 74 (3), 846–861.
Li, J.-Y., Li, T.-Y., Wang, J.-L., Xiang, X.-J., Chen, Y.-X., Li, X., 2013. Characteristics and environmental significance of Ca, Mg, and Sr in the soil infiltrating water overlying the Furong Cave, Chongqing, China. Sci. China Earth Sci. 56 (12), 2126–2134.
Li, T.-Y., Yuan, D.-X., Li, H.-C., Yang, Y., Wang, J.-L., Wang, X.-Y., Li, J.-Y., Qin, J.-M., Zhang, M.-L., Lin, Y.-S., 2007. High-resolution climate variability of southwest China during 57–70 ka reflected in a stalagmite $\delta^{18}O$ record from Xinya Cave. Sci. China (D) 52 (8), 1202–1208.
Li, T.-Y., Han, L.-Y., Cheng, H., Edwards, R.L., Shen, C.-C., Li, H.-C., Li, J.-Y., Huang, C.-X., Zhang, T.-T., Zhao, X., 2017. Evolution of the Asian summer monsoon during Dansgaard/Oeschger events 13–17 recorded in a stalagmite constrained by high-precision chronology from southwest China. Quat. Res. 1–8.
Li, T.-Y., Li, H.-C., Shen, C.-C., Yang, C.-X., Li, J.-Y., Yi, C.-C., Yuan, D.-X., Xie, S.-Y., 2010. Study on the δD and $\delta^{18}O$ characteristics of meteoric precipitation during 2006–2008 in Chongqing. China. Adv. Water Sci. 21 (6), 757–764 (in Chinese).
Li, T.-Y., Shen, C.-C., Huang, L.-J., Jiang, X.-Y., Yang, X.-L., Mii, H.S., Lee, S.Y., Lo, L., 2014. Stalagmite-inferred variability of the Asian summer monsoon during the penultimate glacial–interglacial period. Clim. Past. 10 (3), 1211–1219.
Li, T.-Y., Shen, C.-C., Li, H.-C., Li, J.-Y., Chiang, H.-W., Song, S.-R., Yuan, D.-X., Lin, C.D.-J., Gao, P., Zhou, L.-P., Wang, J.-L., Ye, M.-Y., Tang, L.-L., Xie, S.-Y., 2011. Oxygen and carbon isotopic systematics of aragonite speleothems and water in Furong Cave, Chongqing, China. Geochim. Cosmochim. Acta 75 (15), 4140–4156.
Liu, J., Song, X., Yuan, G., Sun, X., Liu, X., Wang, Z., Wang, S., 2008. Stable isotopes of summer monsoonal precipitation in southern China and the moisture sources evidence from $\delta^{18}O$ signature. J. Geogr. Sci. 18 (2), 155–165 (in Chinese).
Liu, Y.H., Henderson, G.M., Hu, C.-Y., Mason, A.J., Charnley, N., Johnson, K.R., Xie, S.-C., 2013. Links between the East Asian monsoon and North Atlantic climate during the 8,200 year event. Nat. Geosci. 6, 117–120.
Luo, W., Wang, S., 2008. Transmission of oxygen isotope signals of precipitation-soil water-drip water and its implications in Liangfeng Cave of Guizhou, China. Chinese Sci. Bull. 53 (21), 3364–3370.
Maher, B.A., 2008. Holocene variability of the East Asian summer monsoon from Chinese cave records: a re-assessment. Holocene 18 (6), 861–866.
Maher, B.A., Thompson, R., 2012. Oxygen isotopes from Chinese caves: records not of monsoon rainfall but of circulation regime. J. Quat. Sci. 27 (6), 615–624.
Mattey, D.P., Atkinson, T.C., Barker, J.A., Fisher, R., Latin, J.P., Durrell, R., Ainsworth, M., 2016. Carbon dioxide, ground air and carbon cycling in Gibraltar karst. Geochim. Cosmochim. Acta 184, 88–113.
McDermott, F., 2004. Palaeo-climate reconstruction from stable isotope variations in speleothems: a review. Quatern. Sci. Rev. 23 (7), 901–918.
McDonald, J., Drysdale, R., Hill, D., 2004. The 2002–2003 El Niño recorded in Australian cave drip waters: implications for reconstructing rainfall histories using stalagmites. Geophys. Res. Lett. 31 (22), L22202.1–L22202.4.
Mischel, S.A., Scholz, D., Spötl, C., 2015. $\delta^{18}O$ values of cave drip water: a promising proxy for the reconstruction of the North Atlantic Oscillation? Clim. Dynam. 45 (11–12), 3035–3050.
Moerman, J.W., Cobb, K., Partin, J.W., Clark, B., Lejau, S., Malang, J., Tuen, A.A., 2013. Borneo Cave Dripwater Isotope Timeseries Resolve the 2009-2012 ENSO cycle. AGU. Fall M.
Moerman, J.W., Cobb, K.M., Partin, J.W., Meckler, A.N., Carolin, S.A., Adkins, J.F., Lejau, S., Malang, J., Clark, B., Tuen, A.A., 2014. Transformation of ENSO-related rainwater to dripwater $\delta^{18}O$ variability by vadose water mixing. Geophys. Res. Lett. 41 (22), 7907–7915.
Musgrove, M., Banner, J.L., 2004. Controls on the spatial and temporal variability of vadose dripwater geochemistry: edwards Aquifer, central Texas. Geochim. Cosmochim. Acta 68 (5), 1007–1020.
Pape, J.R., Banner, J.L., Mack, L.E., Musgrove, M., Guilfoyle, A., 2010. Controls on oxygen isotope variability in precipitation and cave drip waters, central Texas, USA. J. Hydrol. 385 (1), 203–215.
Partin, J.W., Jenson, J.W., Banner, J.L., Quinn, T.M., Taylor, F.W., Sinclair, D., Hardt, B., Lander, M.A., Bell, T., Miklavič, B., Jocson, J.M.U., Taboroši, D., 2012. Relationship between modern rainfall variability, cave dripwater, and stalagmite geochemistry in Guam. USA. Geochem. Geophys. Geosyst. 13 (3), Q03013.
Pausata, F.S., Battisti, D.S., Nisancioglu, K.H., Bitz, C.M., 2011. Chinese stalagmite $\delta^{18}O$ controlled by changes in the Indian monsoon during a simulated Heinrich event. Nat. Geosci. 4 (7), 474–480.
Peng, H., Mayer, B., Harris, S., Krouse, H.R., 2007. The influence of below-cloud secondary effects on the stable isotope composition of hydrogen and oxygen in precipitation at Calgary, Alberta. Canada. Tellus. B 59 (4), 698–704.
Riechelmann, D.F.C., Schröder-Ritzrau, A., Scholz, D., Fohlmeister, J., Spötl, C., Richter, D.K., Mangini, A., 2011. Monitoring Bunker Cave (NW Germany): a prerequisite to interpret geochemical proxy data of speleothems from this site. J. Hydrol. 409 (3), 682–695.
Riechelmann, S., Schröder-Ritzrau, A., Spötl, C., Riechelmann, D.F.C., Richter, D.K., Mangini, A., Frank, N., Breiteenbach, S.F.M., Immenhauser, A., 2017. Sensitivity of Bunker Cave to climatic forcings highlighted through multi-annual monitoring of rain-, soil-, and dripwaters. Chem. Geol. 449, 194–205.
Sherwin, C.M., Baldini, J.U.L., 2011. Cave air and hydrological controls on prior calcite precipitation and stalagmite growth rates: implications for palaeoclimate reconstructions using speleothems. Geochim. Cosmochim. Acta 75 (14), 3915–3929.
Spötl, C., Fairchild, I.J., Tooth, A.F., 2005. Cave air control on dripwater geochemistry, Obir Caves (Austria): Implications for speleothem deposition in dynamically ventilated caves. Geochim. Cosmochim. Acta 69 (10), 2451–2468.
Sun, J.H., Wei, J., Zhao, S.X., Tao, S.Y., 2006. The weather and its circulation in summer of 2005. Clim. Environ. Res. 11, 138–154 (in Chinese with English abstract).
Tadros, C.V., Treble, P.C., Baker, A., Fairchild, I., Hankin, S., Roach, R., Markowska, M., McDonald, J., 2016. ENSO-cave drip water hydrochemical relationship: a 7-year dataset from south-eastern Australia. Hydrol. Earth Syst. Sci. 20 (11), 4625–4640.
Tan, M., 2014. Circulation effect: response of precipitation $\delta^{18}O$ to the ENSO cycle in monsoon regions of China. Clim. Dynam. 42 (3–4), 1067–1077.
Tan, M., 2016. Circulation background of climate patterns in the past millennium: Uncertainty analysis and re-reconstruction of ENSO-like state. Sci. China Earth Sci. 59 (6), 1225–1241.
Tian, H., Guo, P.W., Lu, W.S., 2004. Characteristics of vapor inflow corridors related to summer rainfall in China and impact factors. J. Trop. Meteorol. 20 (4), 401–408 (in Chinese).
Tian, L.D., Yao, T.D., White, J.W.C., Yu, W.S., Wang, N.L., 2005. Westerly moisture transport to the middle of Himalayas revealed from the high deuterium excess. Chinese Sci. Bull. 50 (10), 1026–1030.

Tooth, A.F., Fairchild, I.J., 2003. Soil and karst aquifer hydrological controls on the geochemical evolution of speleothem-forming drip waters, Crag Cave, southwest Ireland. J. Hydrol. 273 (1), 51–68.
Treble, P.C., Bradley, C., Wood, A., Baker, A., Jex, C.N., Fairchild, I.J., Gagan, M.K., Cowley, J., Azcurra, C., 2013. An isotopic and modelling study of flow paths and storage in Quaternary calcarenite, SW Australia: implications for speleothem paleoclimate records. Quatern. Sci. Rev. 64, 90–103.
Trenberth, K.E., 1997. The definition of El Niño. B. Am. Meteorol. Soc. 78 (12), 2771–2778.
Wackerbarth, A., Scholz, D., Fohlmeister, J., Mangini, A., 2010. Modelling the $\delta^{18}O$ value of cave drip water and speleothem calcite. Earth Planet. Sci. Lett. 299 (3), 387–397.
Wang, H.-B., Li, T.-Y., Yuan, N., Li, J.-Y., 2014. Environmental signification and the characteristics of δD and $\delta^{18}O$ variation in the local precipitation and drip water in Yangkou cave. Chongqing. Carsolog Sin. 33 (2), 146–155 (in Chinese with English abstract).
Wang, Y., Chen, X., Yan, F., 2015. Spatial and temporal variations of annual precipitation during 1960–2010 in China. Quat. Int. 380, 5–13.
Wang, Y.J., Cheng, H., Edwards, R.L., An, Z.S., Wu, J.Y., Shen, C.-C., Dorale, J.A., 2001. A high-resolution absolute-dated late Pleistocene monsoon record from Hulu Cave, China. Science 294 (5550), 2345–2348.
Wang, Y.J., Cheng, H., Edwards, R.L., He, Y.Q., Kong, X.G., An, Z.S., Wu, J.Y., Kelly, M.J., Dykoski, C.A., Li, X.D., 2005. Holocene Asian monsoon: links to solar changes and North Atlantic climate. Science 308 (5723), 854–857.
Wang, Y.J., Cheng, H., Edwards, R.L., Kong, X.G., Shao, X.H., Chen, S.T., Wu, J.Y., Jiang, X.Y., Wang, X.F., An, Z.S., 2008. Millennial-and orbital-scale changes in the East Asian monsoon over the past 224,000 years. Nature 451 (7182), 1090–1093.
Wang, Y.J., Liu, D.B., 2016. Speleothem records of Asian paleomonsoon variability and mechanisms. Chinese Sci. Bull. 61 (9), 938–951.
Wong, C., Banner, J.L., 2010. Response of cave air CO_2 and drip water to brush clearing in central Texas: implications for recharge and soil CO_2 dynamics. J. Geophys. Res. 115 (G4), G04018.
Yang, H., Johnson, K.R., Griffiths, M.L., Yoshimura, K., 2016. Interannual controls on oxygen isotope variability in Asian monsoon precipitation and implications for paleoclimate reconstructions. J. Geophys. Res. 121 (14), 8410–8428.
Yuan, Y., Gao, H., Liu, Y., 2017. Analysis of the characteristics and causes of precipitation anomalies over eastern China in the summer of 2016. Meteor. Mon (in Chinese with English abstract).
Zhang, R., Sumi, A., Kimoto, M., 1999. A diagnostic study of the impact of El Niño on the precipitation in China. Adv. Atmos. Sci. 16 (2), 229–241 (in Chinese).
Zhang, R., Zhu, X., Han, D., Zhang, Y., Fang, F., 1998. Preliminary study on karst caves of MT. Jinfo, Nanchuan. Chongqing. Carsolog. Sin. 17, 196–211 (in Chinese with English abstract).
Zhang, T.-T., Li, T.-Y., Cheng, H., Edwards, R.L., Shen, C.-C., Spötl, C., Li, H.-C., Han, L.Y., Li, J.Y., Huang, C.X., Zhao, X., 2017. Stalagmite-inferred centennial variability of the Asian summer monsoon in southwest China between 58 and 79 ka BP. Quat. Sci. Rev. 160, 1–12.
Zhao, K., Wang, Y., Edwards, R.L., Cheng, H., Liu, D., Kong, X., Ning, Y., 2016. Contribution of ENSO variability to the East Asian summer monsoon in the late Holocene. Palaeogeogr. Palaeoclimatol. Palaeoecol. 449, 510–519.
Zhou, J.-L., Li, T.-Y., 2017. A tentative study of the relationship between annual $\delta^{18}O$ & δD variations of precipitation and atmospheric circulations—a case from Southwest China. Quat. Int.
Zhou, T., Wu, B., Dong, L., 2014. Advances in research of ENSO changes and the associated impacts on Asian-Pacific climate. Asia-Pac. J. Atmos. Sci. 50 (4), 405–422.